

RESEARCH

Open Access



Mechanical Properties and Fire Resistance of 3D-Printed Cementitious Composites with Plastic Waste

Walid Yaqub¹ and Farhad Aslani^{1*}

Abstract

The study focuses on the development of cementitious composites using 3D printing and plastic waste as a sustainable aggregate substitute. This study involves experimenting with various percentages of plastic waste as a partial substitute for ground granulated blast furnace slag (GGBFS) in a control mix. The study examines the anisotropy of the 3D printing process, comparing it with properties of mold-cast samples. In addition, it assesses the fire resistance and mechanical properties of samples at elevated temperatures (100 °C, 300 °C, and 600 °C). Key mechanical properties, including 28-day compressive stress and flexural strength, are determined through experimental testing using a standard compression test and three-point bending test. The study also considers the modulus of elasticity (MOE) in compressive tests to evaluate a sample's ability to deform elastically and the flexural toughness index to assess energy absorption and crack resistance of flexural samples. Following the experimental testing, the study's key findings suggest that significant mass loss occurred at 300 °C and above, with plastic samples demonstrating increased mass loss at 600 °C. At 600 °C, plastic degradation led to the formation of voids and cracks within samples due to heightened internal pressure. Anisotropy was evident in 3D-printed samples, with loads parallel to the layer direction resulting in greater compressive strength and MOE. Furthermore, layer direction parallel to the longitudinal axis of flexural samples yielded higher flexural strength and flexural toughness. Mold-cast samples displayed superior compressive strength and stiffer behavior, with higher MOE compared to 3D-printed samples. However, 3D-printed plastic samples exhibited superior flexural strength compared to mold-cast samples, attributed to the alignment of plastic within the samples. The study also observed a reduction in compressive strength with the addition of plastic, explained by the poor bonding of plastic with cement due to its hydrophobic nature. Despite this, flexural strength generally improved with plastic addition, except at 600 °C, where plastic samples showed significant degradation in both compressive and flexural strength due to plastic degradation within the samples.

Keywords 3D-printed cementitious composites, Mechanical properties, Fire resistance, Plastic waste

1 Introduction

The construction industry drives approximately \$10 trillion in global spending annually, standing as one of the largest sectors worldwide. Despite its economic scale, this industry struggles with notably low productivity compared to others, often due to outdated, inefficient technologies, and its heavy reliance on labor. Concrete construction, in particular, presents intense labor demands and considerable risks for workers. With about 30 billion tons of concrete produced yearly,

Journal information: ISSN 1976-0485 / eISSN 2234-1315.

*Correspondence:

Farhad Aslani
farhad.aslani@uwa.edu.au

¹ Materials and Structures Innovation Group, School of Engineering,
University of Western Australia, Perth, WA 6009, Australia



© The Author(s) 2024. **Open Access** This article is licensed under a Creative Commons Attribution 4.0 International License, which permits use, sharing, adaptation, distribution and reproduction in any medium or format, as long as you give appropriate credit to the original author(s) and the source, provide a link to the Creative Commons licence, and indicate if changes were made. The images or other third party material in this article are included in the article's Creative Commons licence, unless indicated otherwise in a credit line to the material. If material is not included in the article's Creative Commons licence and your intended use is not permitted by statutory regulation or exceeds the permitted use, you will need to obtain permission directly from the copyright holder. To view a copy of this licence, visit <http://creativecommons.org/licenses/by/4.0/>.



Fig. 1 Excessive shrinkage cracking of 3D-printed sample (Schutter et al., 2018)

traditional methods heavily depend on temporary timber formwork, contributing significantly to costs and offering limited reuse value. However, emerging technologies like 3D concrete printing (3DCP) revolutionize this landscape by enabling concrete construction without the need for formwork. Not only does this innovation promise lower costs but it also reduces labor intensity and associated risks, potentially elevating productivity within the concrete construction domain (Sanjayan et al., 2019).

Conversely, the global production of plastic has seen a substantial surge over the past 5 decades, owing to its desirable attributes such as low density, durability, ease of manufacturing, and cost-effectiveness (Ahmad et al., 2022; Karthick et al., 2022). Despite its advantages, approximately 6.5 billion tons of plastic waste are generated worldwide annually, with dismal rates of recycling (Almohana et al., 2022). In Australia alone, a mere 13% of plastic waste was recycled between 2018 and 2019, with a staggering 84% ending up in landfills (National Plastics Plan summary, 2021).

The non-biodegradable nature of plastic poses significant environmental challenges, taking centuries to

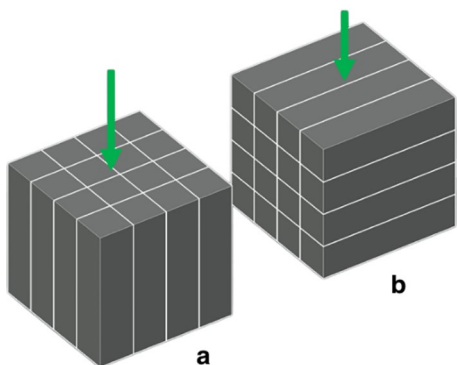


Fig. 2 Compressive 3D-printed sample loading directions

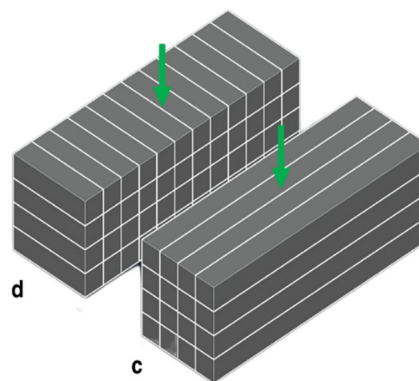


Fig. 3 Flexural 3D-printed sample loading directions

degrade naturally (Almohana et al., 2022). Improper disposal of plastic waste in landfills or as litter not only impacts marine life but also poses health risks to humans and animals due to the release of harmful additives during degradation (Chawla et al., 2022). Furthermore, the degradation of plastics in landfills emits harmful greenhouse gasses, contributing to climate change. Even the incineration of plastic leads to the release of harmful carbon dioxide, exacerbating the issue of climate change (Shen et al., 2020).

Considering these challenges, this paper seeks to explore innovative avenues, such as employing plastic waste in tandem with 3D printing technology, to create sustainable and eco-friendly concrete composites. The challenge of separating plastic from recycled concrete aggregate (RCA) can be addressed through a combination of advanced sorting technologies, mechanical processing, chemical treatments, improved recycling protocols, and innovative uses for plastic-contaminated RCA. In addition, the paper evaluates the fire resistance of these composites to ascertain their durability and mechanical performance when exposed to elevated temperatures. This holistic approach aims to address issues of waste management while advancing sustainable practices in construction and material sciences. To comprehensively assess the mechanical performance of the samples, key parameters such as the 28-day compressive strength, flexural strength, and modulus of elasticity (MOE) for compressive samples, characterizing stiffness, are considered. In addition, the flexural toughness index for all flexural samples, representing ductility and crack resistance, is evaluated. These parameters are pivotal in characterizing the mechanical performance of structural concrete elements. Furthermore, the evaluation of mass loss and the effects of spalling due to exposure to elevated temperatures are also considered to understand the fire resistance of the samples.

Table 1 Previous studies of 3DCP layer direction vs. mold-cast

Mix details	28-day compressive strength results
5% CR by fly ash volume and PVA fibers (Aslani et al., 2022)	7% (direction 'a') and 4% (direction 'b') increase compared to mold cast
Fly ash and silica fume but no fibers (Zahabizadeh et al., 2021)	Up to 18% decrease for 3DCP compared to mold cast. Up to 14% decrease from direction 'a' to direction 'b'
Mix Details	28-day flexural strength results
5% CR by fly ash volume and PVA fibers (Aslani et al., 2022)	158% (direction 'c') and 75% (direction 'd') increase compared to mold cast
PVA fibers (1.5% wt) and activated carbon powder (1% wt) (Zhang & Aslani, 2021)	32% (direction 'c') and 28% (direction 'd') increase compared to mold cast
Fly ash and silica fume but no fibers (Zahabizadeh et al., 2021)	Negligible difference between 3DCP and mold cast. Up to 14% decrease from direction 'c' to direction 'd'

2 Literature Review

2.1 3D Concrete Printing

3D concrete printing (3DCP) stands as a revolutionary technique increasingly integrated into the construction industry (Schutter et al., 2018). Despite the construction industry constituting 13% of global industrial expenditure, its annual growth remains relatively low at 1% (Perrot, 2019). The advent of 3D printing offers the potential for reduced construction costs and waste, along with heightened production efficiency when compared to traditional mold casting methods (Zhang & Aslani, 2021).

To comprehend the challenges inherent in 3D printing, it is essential to consider the general methodology involved (Perrot, 2019). This process begins with digital modeling, where computer-aided design software generates a 3D representation of the structure. Subsequently, this digital model is translated into commands, usually in the form of a G-code—a prevalent programming language for 3D printing operations. The printing process initiates, with the printer utilizing suitable concrete material. Critical to 3DCP is the selection and design of the concrete mix. Given the technique's reliance on

sequentially layering concrete without formwork, factors like the mix's slump and setting time become pivotal. Figure 1 demonstrates how inadequate mix designs with insufficient curing properties can lead to shrinkage cracking, a potential issue associated with 3D printing (Schutter et al., 2018).

While 3D printing a curved structure, tension is anticipated to arise as the material bends along its horizontal plane. If the material's elongation surpasses a critical deformation level, tension-induced breakage and subsequent cracking may occur, especially as the radius of curvature decreases (Perrot, 2019). Consequently, managing the formation of bends during 3D printing of concrete becomes pivotal to prevent crack propagation, preserving the durability and strength of the resulting structure.

To effectively utilize 3DCP as structural components, understanding the mechanical disparities between mold-cast and 3DCP samples is crucial. Given the layer-by-layer printing process inherent in 3D printing, the interface between successive layers significantly influences the product's strength and durability. Anisotropic behavior, where shear loading across layers holds greater

Table 2 Previous studies of plastic addition to concrete

Mix details	Slump results
Plastic waste aggregate (%wt of aggregate) (Ahmad et al., 2022)	30 mm, 100 mm, 120 mm, and 160 mm for 0%, 5%, 15%, and 20% plastic contents, respectively
Plastic fiber (0.25 mm HDPE) reinforcement (% volume of mix) (Pešić et al., 2016)	65 mm, 33 mm, 18 mm, and 13 mm for 0%, 0.5%, 0.75%, and 1.25% fiber contents, respectively
Mix details	28-day compressive strength results
Plastic fine aggregate (%wt of natural sand) (Ali et al., 2021)	42 MPa, 39.1 MPa, 35.8 MPa, and 32.78 MPa for plastic contents 0%, 10%, 15%, and 20%, respectively
Plastic fiber (0.4 mm HDPE) reinforcement (% volume of mix) (Pešić et al., 2016)	33.2 MPa, 31 MPa, 31 MPa, and 30.5 MPa for 0%, 0.4%, 0.75%, and 1.25% fiber contents, respectively
Mix details	28-day flexural strength results
Plastic waste aggregate (%wt of natural sand) (Safi et al., 2013)	10.5 MPa, 8.5 MPa, 6.5 MPa, 7 MPa, and 5.8 MPa for plastic contents 0%, 10%, 20%, 30%, and 50%, respectively
Plastic fiber reinforcement (%wt of mix) (Thiyagarajan, 2013)	4.68 MPa, 4.74 MPa, 4.83 MPa, and 5.06 MPa for 0%, 1%, 2%, and 3% fiber contents, respectively

significance due to weaker inter-layer interfaces, is anticipated in 3D-printed structures (Schutter et al., 2018).

The mechanical properties of a 3D-printed sample are influenced by the direction in which it is loaded, impacted by fiber orientation (if fibers are utilized) and the weaker inter-layer interface. For instance, in compressive loading, a sample may experience force along direction 'a' (parallel to the layer direction) or direction 'b' (perpendicular to the layer direction), as illustrated in Fig. 2. Previous studies using a mix comprising 5% crumb rubber (CR) aggregates as a percentage volume of fly ash and PVA fibers discovered a 3% higher 28-day compressive strength when loaded parallel to direction 'a' compared to loading perpendicular to direction 'b' (Aslani et al., 2022).

A flexural sample can undergo loading in either direction 'c' (print direction parallel to the longitudinal axis of the sample) or 'd' (print direction perpendicular to the longitudinal axis of the specimen), as depicted in Fig. 3. Research conducted on a specific mix design incorporating 5% crumb rubber (CR) aggregates as a percentage volume of fly ash and PVA fibers demonstrated a significant 43% increase in 28-day flexural strength when loaded in direction 'c' compared to direction 'd' (Aslani et al., 2022).

This notable enhancement in flexural strength when loaded in the 'c' direction aligns with expectations, given that fibers oriented along the sample's longitudinal axis exhibit higher tensile capacity along this orientation. In addition, weaker interlocking surfaces between print layers perpendicular to the longitudinal direction, as illustrated in sample 'd,' contribute to reduced flexural strength (Aslani et al., 2022).

Observably, the loading direction exerts a more pronounced influence on the flexural capacity than on the compressive strength of the concrete (cementitious composites) samples. This discrepancy arises due to the increased criticality of interlocking surfaces between print layers in determining flexural capacity.

Understanding the differences in compressive and flexural strength between 3DCP and traditionally mold-cast samples is a critical consideration. Table 1 provides a summary of results obtained from previous studies. The past findings indicate that 3D-printed samples containing fibers exhibit superior compressive strength compared to mold-cast samples, particularly with direction 'a' demonstrating the highest strength. Conversely, mix designs without fibers resulted in reduced compressive strength in 3D-printed samples compared to mold-cast ones. However, direction 'a' still showcased greater strength in the 3D-printed samples. Regarding flexural strength,

Table 3 Previous studies of fire resistance of concrete containing WMP

Mix details	Ambient	200 °C	400 °C	600 °C	800 °C
Concrete composite containing WMP fibers (0.3% volume of mix) (Mohammadosseini et al., 2019)	42 MPa	38 MPa	23 MPa	17 MPa	13 MPa

Table 4 Previous studies of fire resistance of concrete containing PET (Saxena et al., 2018)

Mix details	Compressive strength reduction (Compared to ambient) 300 °C	Compressive strength reduction (Compared to ambient) 600 °C
0% PET	12.36%	26.22%
5% PET	19.16%	35.63%
10% PET	23.83%	47.27%
15% PET	39.13%	55.8%
20% PET	59.26%	64.81%

Table 5 Previous studies of fire resistance of concrete containing CR and fiber reinforcement

Mix details	Mass loss (compared to ambient) 100 °C	Mass loss (compared to ambient) 300 °C	Mass loss (compared to ambient) 600 °C	Mass loss (compared to ambient) 900 °C
Polypropylene fiber-reinforced self-compacting concrete with CR aggregates (Aslani & Kelin, 2018)	Minimal < 1%	Minimal < 1%	Up to 10%	Up to 12%

3D-printed samples using PVA fibers surpassed mold-cast samples, with direction 'c' displaying higher strength. In instances where fibers were absent in the mix design, there was minimal disparity between 3DCP and mold-cast samples, yet direction 'c' still exhibited higher flexural strength compared to direction 'd'. The augmented flexural and compressive strength in 3DCP samples with fibers can be attributed to improved fiber alignment during material extrusion from the nozzle head. In the absence of fibers, the reduction in compressive strength in 3DCP samples occurred due to void formation and the critical impact of weak interfaces between print layers.



Fig. 4 PET plastic wastes

2.2 Plastic Waste in Concrete

Previous studies have indicated that the slump, and consequently the workability of plastic waste used as an aggregate substitute, tends to increase with higher plastic content, as summarized in Table 2. Conversely, a contrasting trend was observed for plastic in fiber form. The increased surface area of plastics from fibers tends to augment friction, consequently reducing slump results. The incorporation of plastic waste as an aggregate substitute leads to a decline in the concrete's compressive strength owing to the hydrophobic nature of plastic, which exhibits poor bonding with cement (Ahmad et al., 2022). Table 2 provides a summary of previous studies investigating the compressive strength of plastic cementitious composites. Notably, the reduction in compressive strength intensifies as the content of plastic in the aggregate increases.

The inclusion of plastic waste significantly impacts the flexural strength of concrete, as evidenced by the findings presented in Table 2 from previous studies. It is notable that while the use of plastic waste as an aggregate substitute decreases compressive strength, its addition in fiber form enhances flexural strength. This enhancement can be attributed to the 'bridging effect,' wherein fibers aligned along the longitudinal axis of a flexural sample effectively resist crack propagation perpendicular to the fibers.

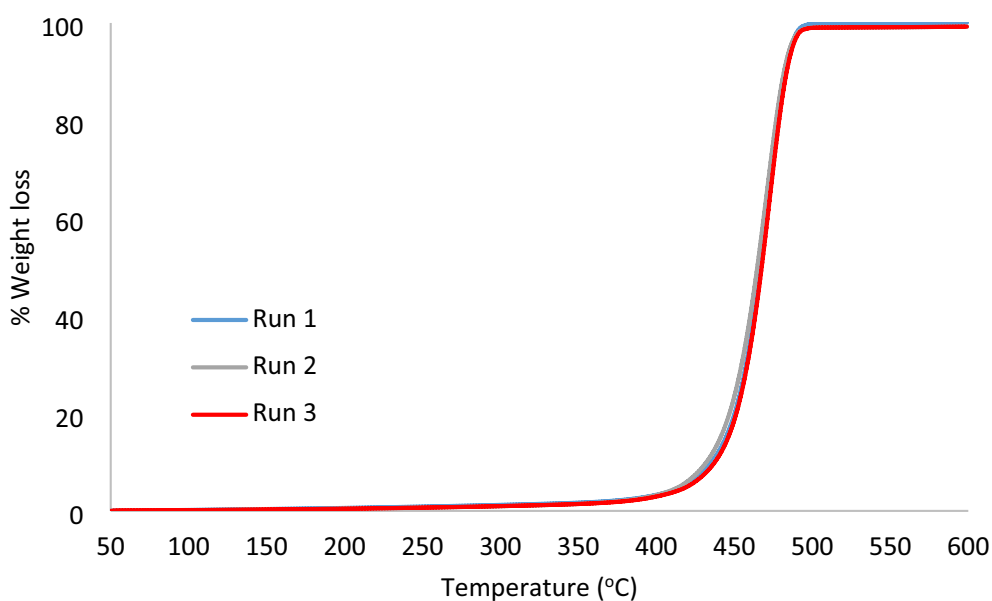


Fig. 5 TGA results for PET plastic wastes

2.3 Fire Resistance of Concrete

Understanding how mechanical properties of concrete composites change when exposed to elevated temperatures is crucial for assessing durability. In a previous experiment examining sustainable concrete utilizing WMP (waste metallized plastic) fibers, the 28-day compressive strength results are collated in Table 3. At 200 °C, there was minimal loss in compressive strength attributed to the partial loss of free water. However, temperatures exceeding 400 °C led to a sharp decline in compressive strength due to the vaporization of bound water (Mohammadhosseini et al., 2019).

A separate study investigated the utilization of polyethylene terephthalate (PET) plastic waste, shredded into fine aggregate as a partial substitute (%wt of mix) (Saxena et al., 2018). The 28-day compressive strengths' outcomes are summarized in Table 4. The study reveals that incorporating PET plastic waste as an aggregate substitute results in a greater loss of compressive strength compared to samples without PET. This behavior is attributed to the thermal degradation of PET, causing increased voids and thermal stress within the sample (Saxena et al., 2018). Notably, at 600 °C, the compressive strengths exhibited a larger decline compared to 300 °C, aligning with the expected degradation of PET occurring at temperatures exceeding 300 °C.

The response of concrete to elevated temperatures includes observed mass loss and visible spalling effects. Spalling, characterized by visible cracks and surface pitting, occurs when concrete is exposed to high temperatures, leading to sample degradation. A prior study examined fiber-reinforced self-compacting concrete containing crumb rubber aggregates under elevated temperatures, and the findings are summarized in Table 5. Minimal mass loss was noted at 100 °C and 300 °C. However, at 600 °C and 900 °C, a significant increase in mass loss was observed. In addition, spalling effects became apparent at these temperatures, characterized by surface cracking and pitting. The heightened mass loss at these elevated temperatures is attributed to the evaporation of both chemically bound and free waters in the samples, consequently increasing internal pressures and causing spalling (Aslani & Kelin, 2018).



Fig. 6 HC1008 desktop 3D printer

3 Experimental Study

3.1 Materials

3.1.1 Cement

This research employed general purpose cement (GPC) conforming to AS 3972 (2010) Type GP for its experimental phase. GPC is crafted from a blend of Portland cement clinker, gypsum, and limestone.

3.1.2 Ground Granulated Blast Furnace Slag

Ground granulated blast furnace slag (GGBFS) serves as an additional cementitious material, functioning as another type of pozzolan. Its application can prolong setting time, and though its initial strength gain is typically slower, it leads to greater overall strength in later stages. The GGBFS utilized in this context was procured from BCG and adheres to AS 3582.2 (2001).

3.1.3 Silica Fume

The silica fume employed in this study underwent testing following AS3582.3 (1994) standards. Comprised of ultra-fine spherical glass particles, silica fume exhibits a finer texture compared to cement particles. Its amplified surface area enhances reactivity, facilitating notable early strength gain, diminishing concrete permeability, and minimizing the likelihood of bleeding.

Table 6 Mix proportions

Name	Water / binder ratio	Portland cement	GGBFS	Densified silica fume	45/ 50 silica sand	Plastic
CM	0.33	1	1.2	0.11	1.68	0
PL5%	0.33	1	1.14	0.11	1.68	0.043
PL10%	0.33	1	1.08	0.11	1.68	0.086
PL15%	0.33	1	1.02	0.11	1.68	0.129
PL20%	0.33	1	0.96	0.11	1.68	0.172

3.1.4 Fine Sand

In this experiment, Fine AFS 45–50 silica sand was utilized. Sampling methods and aggregate testing were conducted in compliance with AS 1141 (2011) standards.

3.1.5 Plastic Waste Aggregates

In this study, less than 2 mm size of polyethylene terephthalate (PET) plastic wastes have been used (see Fig. 4). The thermal decomposition behavior of PET plastic waste samples as indicated by the rate of mass loss during continuous heating was measured using a thermogravimetric analyzer (TGA, TA Instrument Q5000IR). A thin layer of the sample (around 5–8 mg) was placed at the center of the sample crucible and loaded in the TGA. The sample was first equilibrated at 50 °C and then heated at 10 °C min⁻¹ from 50 °C to the final temperature. During the heating, the mass and temperature of the sample were continuously recorded. High-purity nitrogen was used as a purge gas at a constant flow rate of 100 ml min⁻¹. The weight loss of specimens vs. temperature is plotted in Fig. 5. TGA results revealed the temperature at which degradation starts and the range in which a weight loss of 90% was achieved. However, PET plastic waste samples showed 100% weight loss at a temperature of 495 °C.

3.1.6 Chemical Admixtures

In this experiment, the superplasticizer (SP) meets the criteria of AS 1478.1 (2000) as a type SN chemical admixture. Its purpose is to decrease the viscosity and yield

stress of fresh concrete, enhancing the concrete’s flow properties. The high-range water reducer (HRWR) meets the specifications of Type HWR under AS1478.1 (2000). In addition, the viscosity-modifying admixture (VMA) employed in this study aligns with AS1478 (2000) standards for type SN admixtures, crucial for controlling stability and resistance to segregation in mortar.

3.2 Mix Proportions

In line with the research objectives, the study is structured into two primary sections: (i) the preparation and testing of mold-casted specimens, and (ii) the creation of identical specimens through 3DCP technology. This approach aims to offer comprehensive insights into the impact of 3DCP technology on the mechanical characteristics of plastic-based concrete, contrasting its effects with conventional casting methods. Five mix designs were formulated and blended following the guidelines outlined in AS 1012.2 (1994), specifying the appropriate laboratory protocols for preparing concrete mixes (see Table 6).

3.3 Sample Preparation and Curing Conditions

Specimens underwent casting and curing procedures according to their respective standards: AS 1012.8.1 (2014) for compression and flexural test samples. The standard entails similar casting methods, involving pouring wet concrete into appropriately lubricated molds as specified, then compacting the mixture using a vibrating table to eliminate potential air voids. Three specimens

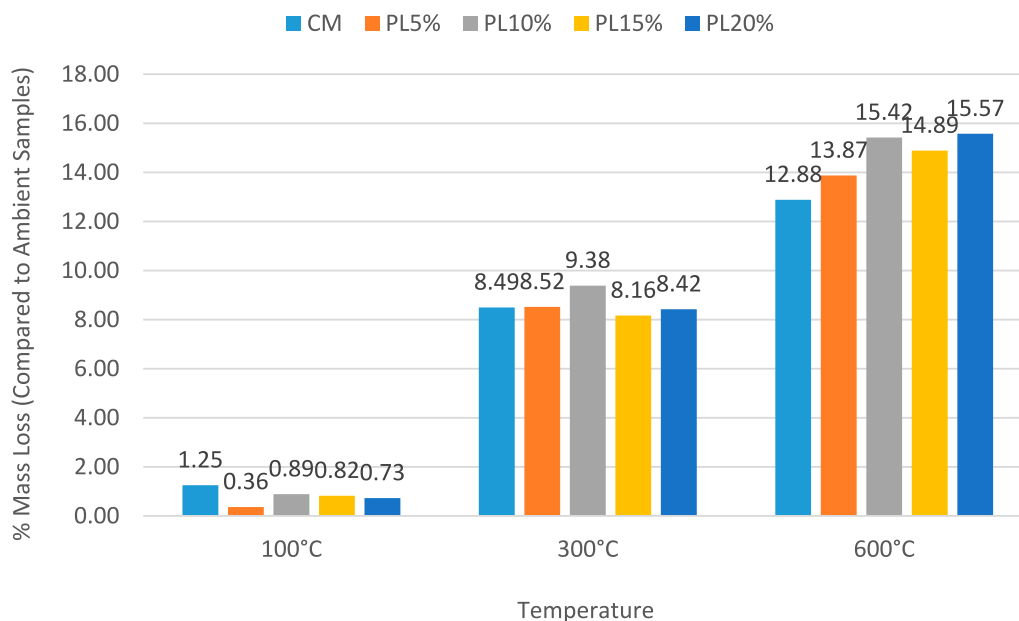










Fig. 7 Mass loss of mixes

Table 7 Spalling of mixes

	CM	PL
Ambient		
100°C		
300°C		
600°C		

for each of the six mix designs were prepared, with mold dimensions of 50 mm for compression tests and 50×50×150 mm for flexural tests.

Following casting, initial curing commenced by placing the molds on a horizontal surface at 23±2 °C for 24 h. Subsequently, the specimens were demolded and subjected to standard moist curing conditions until testing. This curing process is critical for proper cement hydration, ensuring appropriate development of the mixture properties.

For the assessment of the exclusive impact of 3DCP technology on compressive and flexural performance, 3D-printed specimens were generated using the HC1008 Desktop Concrete 3D Printer (Fig. 6). The selection of this printer was based on its precision, speed, and suitability for plastic-based concrete. Unlike the cast samples, the 3D-printed specimens were created as cuboid structures, later manually cut to the required test sample sizes. Schematics depicting the cuboid structures and cutting orientations of printed samples. Prior to printing, codes were created to instruct the 3D printer on the desired geometries. To assess the influence of print direction on mechanical and shrinkage performance, two print

directions were tested for each test type, necessitating the creation of six codes.

The process for constructing the 3D-printed cuboids involved running the printing code and pouring the wet concrete mixture into the printer funnel, allowing for layer-by-layer construction. Due to the absence of a mold, vibration to release air pockets was not feasible during printing; thus, air pocket release relied on mechanically applied pressure during extrusion. Similarly, gauge studs could not be inserted into the specimens for shrinkage tests due to the absence of attachment points.

3.4 Testing Methods

3.4.1 Mass Loss and Spalling

The mass of concrete decreases as temperature rises due to moisture loss. The retention of mass in concrete at elevated temperatures is strongly influenced by the type of aggregate used. Mass measurements of the specimens before and after exposure to high temperatures were conducted according to AS 1012.12.1 (1998).

Spalling, defined as the detachment of parts of concrete from the surface when subjected to high temperatures, was observed. After heating, the samples were visually

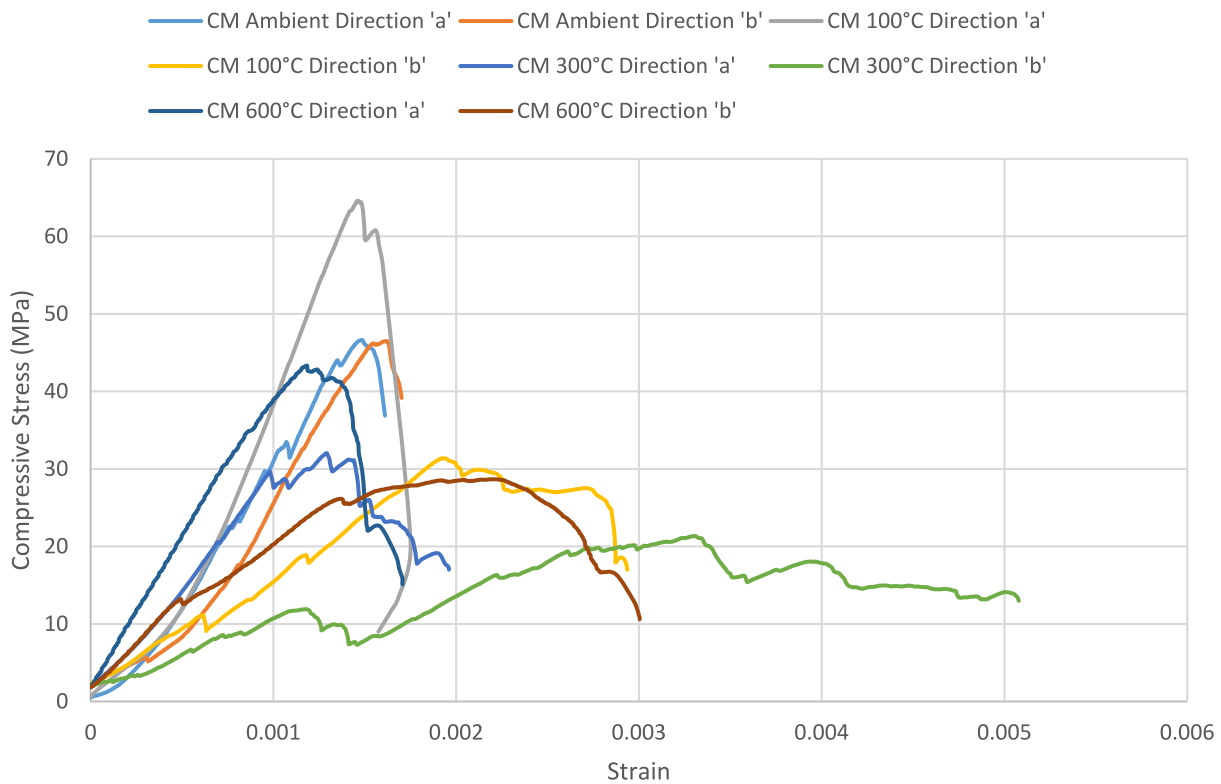


Fig. 8 The effect of 3DCP layer direction on compressive stress–strain curves

Table 8 The effect of 3DCP layer direction on MOE results

Sample type	Peak stress (MPa)	Peak strain	Strain at 40% peak stress	MOE (GPa)
CM 3DCP ambient direction 'a'	46.6	0.00161	0.00066	28.2
CM 3DCP ambient direction 'b'	46.5	0.00170	0.00084	22.0
CM 3DCP 100 °C direction 'a'	64.6	0.00175	0.00079	32.9
CM 3DCP 100 °C direction 'b'	31.4	0.00294	0.00082	15.3
CM 3DCP 300 °C direction 'a'	32.0	0.00196	0.00045	28.3
CM 3DCP 300 °C direction 'b'	21.4	0.00508	0.00078	11.0
CM 3DCP 600 °C direction 'a'	43.3	0.00171	0.00040	43.1
CM 3DCP 600 °C direction 'b'	28.7	0.00300	0.00040	28.5

inspected for the formation of cracks, bubbles, holes, and loss of material. Subsequently, spalling measurements of the specimens were carried out after exposure to high temperatures.

3.4.2 Mechanical Properties

Before initiating the 28-day compressive strength assessment, the cubic samples underwent weighing to determine the mixture density. Subsequently, the Instron 5982 loading machine was utilized for both 7- and 28-day compressive strength tests, as well as three-point bending

tests, all conducted under displacement-controlled conditions. These tests maintained a loading rate of 1 mm per minute, with a span length of 122.5 mm for the three-point bending examination.

The effect of elevated temperatures on mechanical properties of the mixtures was measured by heating the cylinders at 5 °C/min to temperatures of 100, 300, and 600 °C. This was kept for 1 h, and the samples were then slowly cooled to room temperature for 24 h before the residual strength tests were conducted.

Table 9 Compressive sample failure modes in 3DCP layer orientation

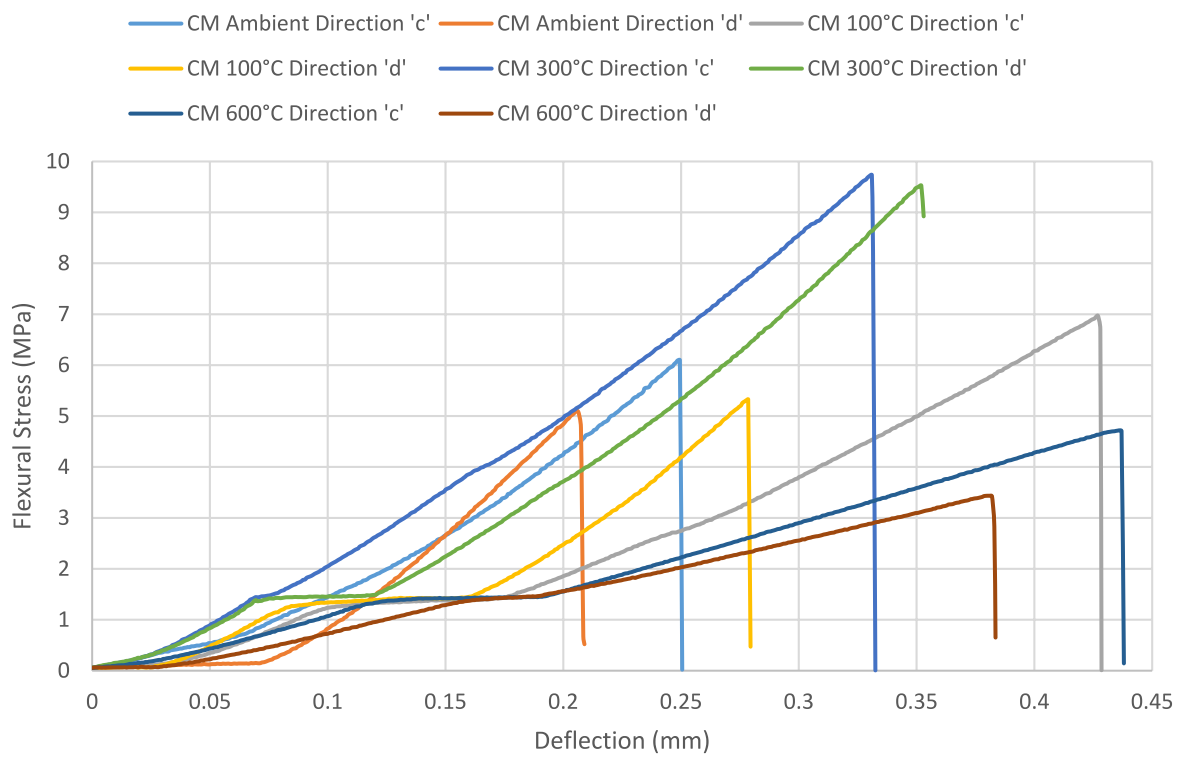
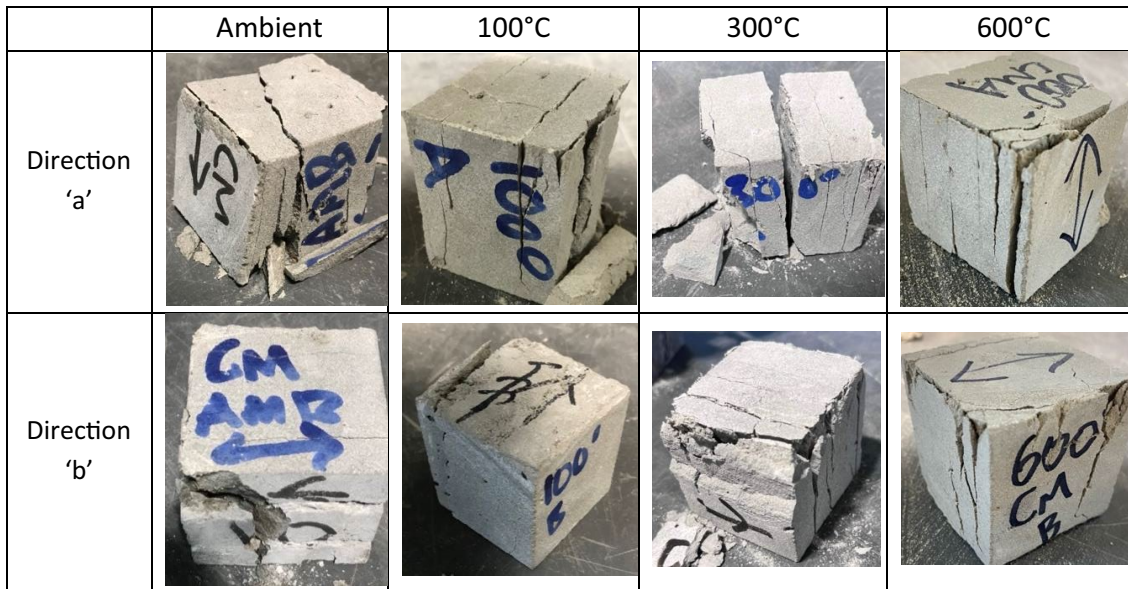


Fig. 9 The effect of 3DCP layer direction on flexural stress–deflection curves

Table 10 The effect of 3DCP layer direction on flexural toughness

Sample type	Post-peak energy $E_{L/m}$ (N.m)	Peak deflection (mm)	PCS ₁₅₀ (MPa)
CM 3DCP ambient direction 'c'	0.211	0.249	0.718
CM 3DCP ambient direction 'd'	0.118	0.206	0.373
CM 3DCP 100 °C direction 'c'	0.410	0.427	2.063
CM 3DCP 100 °C direction 'd'	0.186	0.279	0.668
CM 3DCP 300 °C direction 'c'	0.500	0.331	1.999
CM 3DCP 300 °C direction 'd'	0.463	0.352	1.937
CM 3DCP 600 °C direction 'c'	0.333	0.436	1.716
CM 3DCP 600 °C direction 'd'	0.215	0.381	0.960

To explore the impact of anisotropy on 3D-printed specimens, evaluations of compressive and flexural strength were conducted in distinct directions. In the compressive strength test, loading occurred along a and b directions (as shown in Fig. 2), aligning with loading parallel and perpendicular to the fiber direction, respectively. As for the flexural strength test, loading took place in c and d directions (illustrated in Fig. 3), reflecting the orientation of fibers within the specimen, aligning parallel and perpendicular to the longitudinal axis of the specimen, respectively.





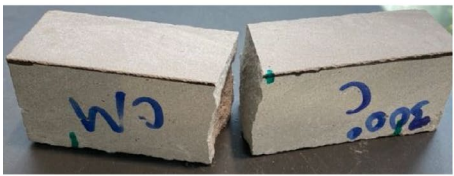



4 Experimental Results

4.1 Mass Loss and Spalling

Figure 7 illustrates the percentage mass loss of samples relative to ambient conditions, while Table 7 details the physical effects observed during heating.

The control mix (CM) samples exhibited no visible formation of cracks or signs of spalling across all temperature ranges. At 600 °C, CM samples displayed slight discoloration due to the evaporation of bound waters and felt chalkier to the touch. Plastic samples showed no discernible effects of heating at 100 °C. Upon reaching 300 °C, all plastic samples exhibited surface discoloration

Table 11 Flexural sample failure modes in 3DCP layer orientation

	Direction 'c'	Direction 'd'
Ambient		
100°C		
300°C		
600°C		

in areas containing plastic, accompanied by some thermal expansion evidenced by bulging of the plastic particles. At this temperature, light surface cracking was observed on certain samples, although no significant pits or cracks were detected. However, upon reaching 600 °C, evident physical effects of spalling were observed across all plastic samples. Degradation of the plastic resulted in void formation within the concrete and discoloration of the samples. In addition, considerable cracking was evident on all plastic samples due to the increased internal pressure. Such degradation of plastic samples at this

temperature was anticipated, as plastic waste typically undergoes complete degradation between 400 °C and 550 °C, depending on its composition (Singh et al., 2019).

The results indicate that negligible mass loss, below 1.25%, was observed at 100 °C for all samples. At 300 °C, significant mass loss ranging from 8.16% to 9.38% occurred due to the evaporation of water from the samples. Upon reaching 600 °C, mass loss increased considerably, ranging from 12.88% to 15.57%, attributed to the evaporation of both chemically bound and free waters. There is a clear positive correlation between

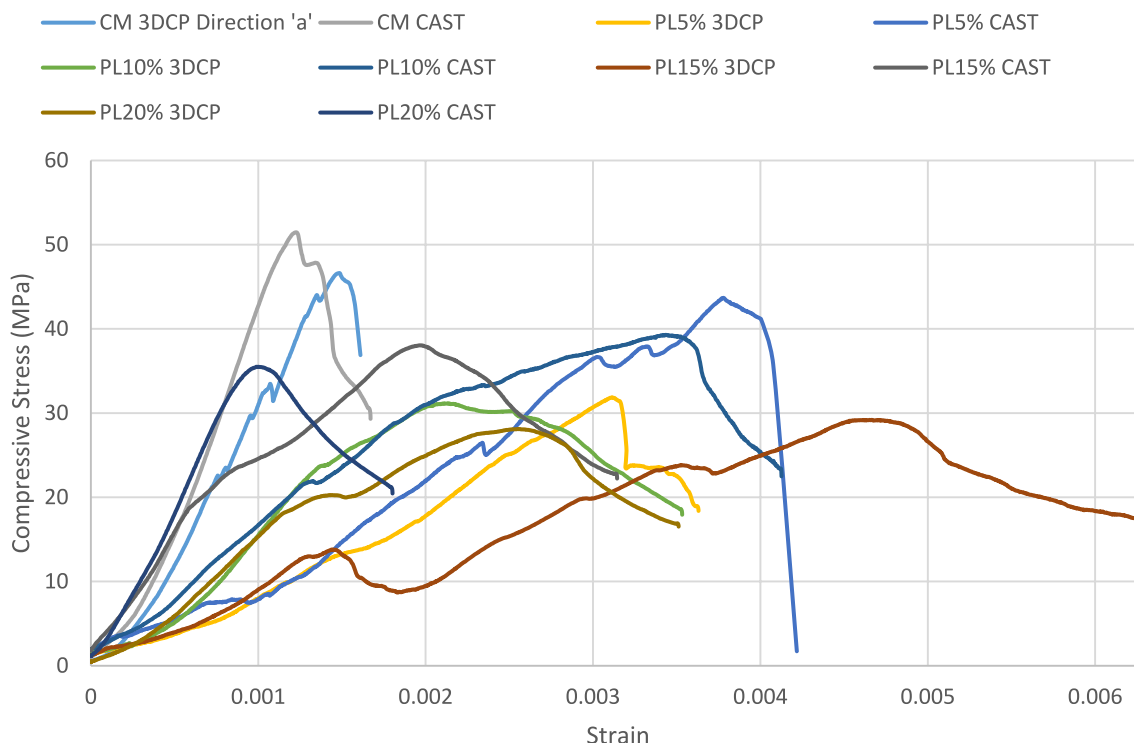












Fig. 10 The effect of mold-cast vs. 3DCP on compressive stress–strain curves

Table 12 The effect of mold-cast vs. 3DCP on MOE results

Sample type	Peak stress (MPa)	Peak strain	Strain at 40% peak stress	MOE (GPa)
CM 3DCP ambient direction 'a'	46.6	0.00161	0.00066	28.2
CM Cast ambient	51.5	0.00167	0.00061	34.0
PL5% 3DCP ambient	43.7	0.00363	0.00143	12.2
PL5% cast ambient	39.3	0.00422	0.00167	9.4
PL10% 3DCP ambient	38.0	0.00353	0.00087	17.4
PL10% cast ambient	35.5	0.00413	0.00094	15.1
PL15% 3DCP ambient	31.9	0.00626	0.00118	10.8
PL15% cast ambient	31.2	0.00314	0.00048	26.1
PL20% 3DCP ambient	29.2	0.00351	0.00078	14.9
PL20% cast ambient	28.1	0.00180	0.00041	27.4

Table 13 Compressive sample failure modes in mold-cast vs. 3DCP

	CM Direction 'a'	PL5%	PL10%	PL15%	PL20%
3D Printed					
Mould Cast					

increasing plastic content and mass loss at 600 °C, indicative of a greater loss of plastic mass as it degraded at this temperature.

4.2 Mechanical Properties of 3D-Printed Samples Optimal Layer Direction

4.2.1 Compressive Strength Results of Control Mix

The effects of 3D printing layer orientation have been considered for CM samples across all temperature ranges to ascertain the optimal loading direction.

The results for compressive stress–strain curves, peak compressive strengths, and MOE are presented in Fig. 8 and Table 8, respectively. The failure modes of 3D-printed compressive samples in direction 'a' with the load parallel to the layer direction or direction 'b' with the load perpendicular to the layer direction are detailed in Table 9. In compressive tests, the MOE is typically calculated by determining the slope of the linear region of the stress–strain curve up to the strain corresponding to when 40% of the peak stress is reached (Aslani et al., 2022).

The results across all temperature ranges indicate that direction 'a' exhibits superior compressive strength, with an average 51.8% increase compared to direction 'b'. These findings are consistent with prior studies discussed in the literature review, which anticipated higher compressive strength in direction 'a'. In addition, it was observed that direction 'a' generally exhibited higher MOE across all samples except at ambient temperature, consistent with results from a previous study that considered fly ash and silica fume but no fibers in the mix design (Zahabizadeh et al., 2021). This suggests that samples loaded in direction 'a' displayed stiffer (less ductile) behavior. This behavior was further evidenced by lower peak strains observed in all samples loaded in direction 'a'.

The failure mode for compressive samples loaded in the direction 'a' showed non-explosive shear failure planes forming parallel to the loading direction between different print layers. This was particularly evident in the 300 °C direction 'a' sample, where a clear failure plane ran through the middle of the sample between print layers. Samples loaded in direction 'b', however, exhibited cracking of the outer faces of the cubes rather than failure planes running through the center of the samples.

4.2.2 Flexural Strength Results of Control Mix

The flexural stress–deflection curves, peak flexural strengths, and flexural toughness index results are presented in Fig. 9 and Table 10, respectively. Table 11 displays the failure modes of 3D-printed flexural samples with print layers aligned parallel (direction 'c') or perpendicular (direction 'd') to the prism's longitudinal axis. The flexural toughness index serves as a metric for evaluating a material's capacity to absorb energy and resist crack propagation (ductility). A higher flexural toughness index indicates that a sample can endure more deformation and absorb greater energy before reaching failure. This index is typically assessed by considering the post-crack strength (PCS_m), constrained to a specific deflection (L/m), where 'm' is typically taken as an arbitrary value, often set to 150 (Zhang & Aslani, 2021).

$$PCS_m = \frac{(E_{post,m})L}{(\frac{L}{m} - \delta_{peak})bh^2} \tag{1}$$

where : $E_{post,m} = \text{Post - peak energy to limit } L/m \text{ (Area under load deflection plot)}$,
 $\delta_{peak} = \text{Deflection at peak load}$, $m = 150$, $L/m = \frac{120}{150} = 0.8mm$

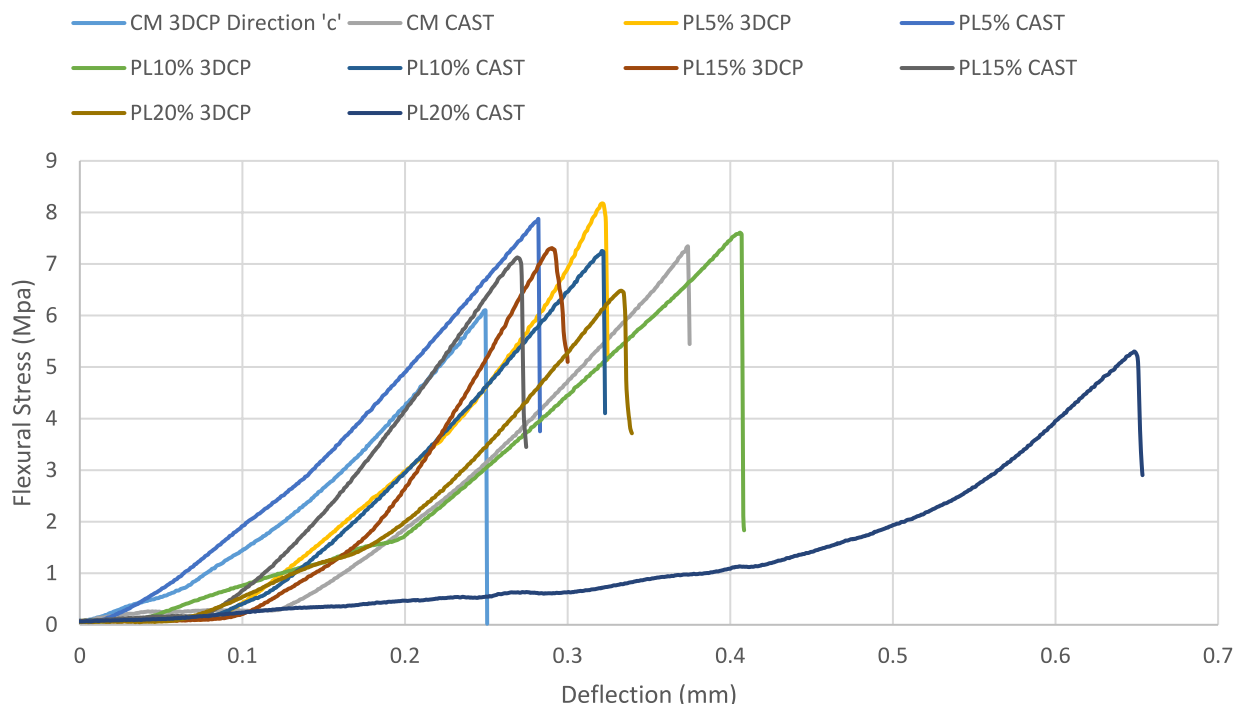


Fig. 11 The effect of mold-cast vs. 3DCP on flexural stress–deflection curves

Table 14 The effect of mold-cast vs. 3DCP on flexural toughness

Sample type	Post-peak energy $E_{L/m}$ (N.m)	Peak deflection (mm)	PCS_{150} (MPa)
CM 3DCP ambient Direction 'c'	0.211	0.249	0.718
CM cast ambient	0.311	0.374	1.371
PL5% 3DCP ambient	0.297	0.321	1.163
PL5% cast ambient	0.333	0.282	1.205
PL10% 3DCP ambient	0.395	0.406	1.880
PL10% cast ambient	0.280	0.321	1.098
PL15% 3DCP ambient	0.227	0.291	0.835
PL15% cast ambient	0.238	0.269	0.839
PL20% 3DCP ambient	0.255	0.333	1.024
PL20% cast ambient	0.305	0.649	3.778

The results indicate that direction 'c' demonstrates superior flexural strength across all temperatures, with an average 22.3% increase compared to direction 'd'. These findings are consistent with previous studies outlined in the '3D Printing Concrete Overview', where direction 'c' was expected to exhibit superior flexural strength. The increase in flexural strength for direction 'c' can be attributed to weaker print layer interfaces becoming critical in direction 'd', thereby reducing the flexural strength of these samples. Brittle failure mode was observed for

all samples, characterized by a sharp drop in load after reaching peak strength. Direction 'c' exhibited greater flexural toughness, resulting in improved crack resistance (ductility), as evidenced by higher PCS_{150} for all samples in direction 'c' compared to 'd' across all temperature ranges. These findings align with the results of a previous study considering CR aggregates and PVA fibers (Aslani et al., 2022).

The failure mode for flexural samples with layer directions 'c' and 'd' remained consistent between both orientations. It was observed that some samples with layer orientation 'd' experienced failure planes away from the midspan, particularly evident in the 300 °C sample. This phenomenon can be attributed to crack propagation occurring between weaker print layer interfaces.

4.3 Mechanical Properties of Mold-Cast vs. 3D-Printed Samples

Mold-cast and 3D-printed samples were produced for both cementitious material and waste plastic at ambient temperature to compare their mechanical performance. Based on the results from the previous section, plastic samples were exclusively tested in the optimal directions 'a' and 'c' for compressive and flexural tests, respectively. These orientations demonstrated superior compressive and flexural strengths.

Table 15 The effect of mold-cast vs. 3DCP on flexural sample failure modes











	3D Printed	Mould Cast
CM		
PL5%		
PL10%		
PL15%		
PL20%		



Fig. 12. 3D-printed flexural sample plastic alignment

4.3.1 Compressive Strength

The results for compressive stress–strain curves, peak compressive strengths, and MOE are depicted in Fig. 10

and Table 12, respectively. In addition, the failure modes of the compressive samples are summarized in Table 13.

The results indicate that mold-cast samples demonstrate superior compressive strength across all mix designs, with an average 26% increase compared to 3D-printed samples. These findings are consistent with prior studies where mold-cast samples without fibers typically exhibit higher compressive strength than 3D-printed ones. The decline in compressive strength with 3D-printed samples can be attributed to weaker print interfaces and the formation of voids during printing, which can be minimized in mold casting through vibration to remove voids.

Mold-cast samples also demonstrated stiffer and less flexible behavior, showing an average 42% increase in MOE compared to 3D-printed samples. This aligns with findings from previous studies that considered mix designs with CR aggregates and PVA fibers (Aslani et al., 2022).

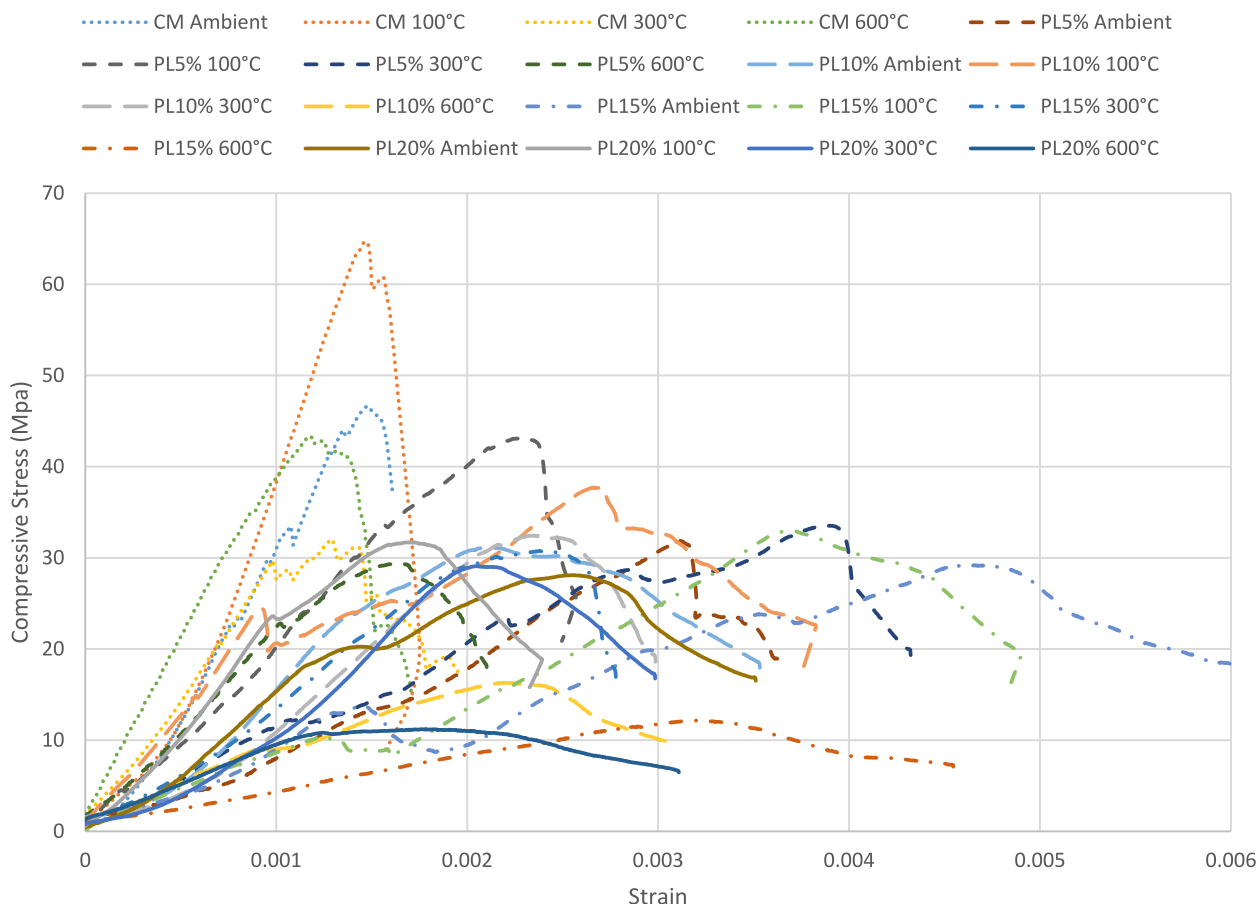


Fig. 13 The effects of elevated temperature and plastic addition on compressive stress–strain curves

Mold-cast samples typically exhibited shear cracking on the outer faces without significant shear failure planes forming in the centers. In contrast, the 3D-printed cementitious material sample failed along a shear plane running through its center, likely propagated between print layers. The 3D-printed plastic samples consistently failed, with patterns similar to their respective mold-cast counterparts, displaying shear cracking on the outer faces.

4.3.2 Flexural Strength

The results for flexural stress–deflection curves, peak flexural strengths, and flexural toughness index are summarized in Fig. 11 and Table 14, respectively. In addition, the failure modes of the flexural samples are illustrated in Table 15.

The mold-cast cementitious material sample demonstrated superior flexural strength, exhibiting a 20.3% increase compared to the 3D-printed sample. This observation suggests that the 3D printing process does not inherently yield greater flexural strength, especially in the absence of fibers in the mix design, which could

enhance ‘bridging’ effects and resist crack propagation. Conversely, plastic mold-cast samples showed an average 7.2% decrease in flexural strength compared to 3D-printed samples. Despite the plastic being in aggregate form, it is likely that some of the longer strands aligned with the longitudinal axis of the flexural prisms during the 3D printing process, leading to increased flexural strength, as depicted in Fig. 12. Post-crack strength at a deflection of 150 mm was greater for all mold-cast samples (excluding PL10%), indicating greater ductility and flexural toughness compared to 3D-printed samples.

The failure modes observed in both mold-cast and 3D-printed samples were consistent, characterized by brittle failure exhibited in stress–deflection plots with a rapid drop from peak load. Notably, the 3D-printed samples with 15% and 20% plastic content, along with the mold-cast sample with 15% plastic content, did not completely split into two pieces upon testing completion, but visible crack propagation was evident from the tensile region of the samples.

Table 16 The effects of elevated temperature and plastic addition on MOE results

Sample type	Peak stress (MPa)	Peak strain	Strain at 40% peak stress	MOE (GPa)
CM 3DCP ambient direction 'a'	46.6	0.00161	0.00066	28.2
PL5% 3DCP ambient	43.7	0.00363	0.00143	12.2
PL10% 3DCP ambient	38.0	0.00353	0.00087	17.4
PL15% 3DCP ambient	31.9	0.00626	0.00118	10.8
PL20% 3DCP ambient	29.2	0.00351	0.00078	14.9
CM 3DCP 100 °C direction 'a'	64.6	0.00175	0.00079	32.9
PL5% 3DCP 100 °C	43.1	0.00257	0.00089	19.4
PL10% 3DCP 100 °C	37.7	0.00383	0.00061	24.9
PL15% 3DCP 100 °C	33.0	0.00490	0.00198	6.7
PL20% 3DCP 100 °C	31.7	0.00239	0.00059	21.4
CM 3DCP 300 °C direction 'a'	32.0	0.00196	0.00045	28.3
PL5% 3DCP 300 °C	33.5	0.00432	0.00140	9.6
PL10% 3DCP 300 °C	32.4	0.00299	0.00111	11.7
PL15% 3DCP 300 °C	30.8	0.00278	0.00093	13.2
PL20% 3DCP 300 °C	29.1	0.00298	0.00109	10.6
CM 3DCP 600 °C direction 'a'	43.3	0.00171	0.00040	43.1
PL5% 3DCP 600 °C	29.4	0.00213	0.00054	21.6
PL10% 3DCP 600 °C	16.3	0.00308	0.00062	10.6
PL15% 3DCP 600 °C	12.1	0.00455	0.00113	4.3
PL20% 3DCP 600 °C	11.2	0.00311	0.00042	10.7

4.4 Effects of Plastic Waste Content on Concrete and Its Response to Elevated Temperatures

The mechanical properties of concrete samples containing various levels of plastic percentage replacement are outlined in this section, along with their response to elevated temperatures compared to control mix samples. It should be noted that the plastic samples have only been tested in optimal directions 'a' and 'c' for compressive and flexural tests, respectively, as these orientations demonstrated superior compressive and flexural strengths as outlined earlier.

4.4.1 Compressive Strength

The results for compressive stress–strain curves, peak compressive strengths, and MOE are depicted in Fig. 13 and Table 16. The failure modes of compressive samples are presented in Table 17.





















Experimental results indicate that the addition of plastic waste in samples resulted in a reduction of compressive strength across all temperatures compared to the samples. Furthermore, it is evident that increasing plastic content correlates with further reductions in compressive strength. These findings are consistent with previous studies outlined in Table 7, as significant compressive

strength loss with samples containing plastics is expected due to the hydrophobic nature of plastic, which bonds poorly with cement.

In addition, experimental results demonstrate that all mix types exhibited superior compressive strength at 100 °C, at which the mass loss was considered insignificant. The fire resistance of the samples was superior, with a 7.1% difference in compressive strength between the ambient and 600 °C samples. Conversely, plastic samples exhibited an average 43.5% drop in compressive strength from ambient to 600 °C.

The MOE for all samples surpassed that of plastic samples at all temperatures, indicating that samples exhibited stiffer and less flexible behaviors. This observation was consistent with samples demonstrating lower peak strain across all temperature ranges compared to plastic samples. The response of MOE across different temperatures yielded varied results. PL5%, PL10%, and PL20% samples exhibited peak MOE at 100 °C, a behavior also observed in a past study considering a mix design with CR aggregates and polypropylene fibers (Aslani & Kelin, 2018). However, at higher temperatures, MOE decreased considerably, as observed with PL10%, PL15%, and PL20% samples exhibiting minimum MOE values at 600 °C,

Table 17 The effects of elevated temperature and plastic addition on compressive sample failure modes

	CM Direction 'a'	PL5%	PL10%	PL15%	PL20%
Ambient					
100°C					
300°C					
600°C					

contrary to samples, which had peak MOE at this temperature, an unexpected outcome.

The failure mode for compressive plastic samples at temperatures ranging from ambient to 300 °C was consistent, with shear failure planes forming on the outer faces of the samples. Conversely, samples from ambient to 600 °C exhibited shear failure planes occurring more centrally within the samples. At 600 °C, the plastic samples displayed considerable surface cracking and voids prior to testing, leading to more explosive failure modes.

4.4.2 Flexural Strength

Summary of results for flexural stress–deflection curves, peak flexural strengths, and flexural toughness index is provided in Fig. 14 and Table 18. The failure modes of flexural samples are depicted in Table 19.

Overall, plastic samples generally demonstrated higher flexural strength compared to CM samples across all temperatures excluding 600 °C, with PL5% exhibiting superior strength. The enhanced flexural properties of the plastic samples can be attributed to the alignment of plastic within the samples, as depicted in Fig. 12. Non-brittle failure modes were observed for PL15% and PL20% at 100 °C, characterized by a slow drop-off from peak load rather than an instantaneous drop. Plastic samples at all percentages and temperatures (excluding

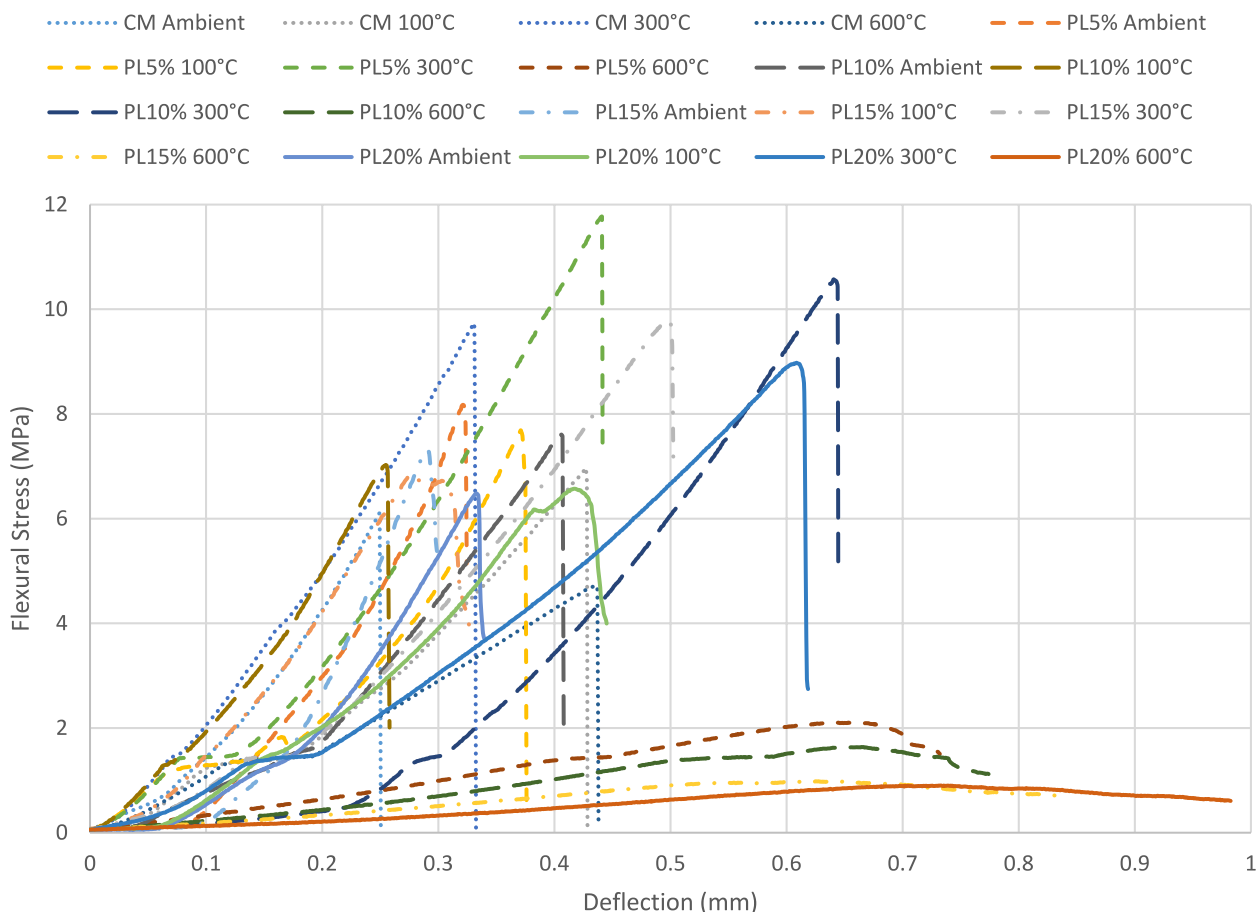


Fig. 14 The effects of elevated temperature and plastic addition on flexural stress–deflection curves

100 °C) exhibited higher flexural toughness and ductility compared to CM samples, as evidenced by higher PCS150 values. This behavior aligns with a past study considering a mix design with activated carbon powder and the use of PVA fibers, where samples containing PVA fibers demonstrated higher flexural toughness compared to samples without PVA fibers (Zhang & Aslani, 2021). The improved bridging effect with the addition of plastics enhances resistance to flexural crack propagation. Plastic-reinforced concrete exhibits better bridging effect and toughness due to the effective crack bridging by randomly distributed plastic fibers, their tensile strength, energy absorption, and the ductile behavior of the fibers during deformation.

Interestingly, flexural strength of samples at 300 °C was superior across all mix types, contrary to expectations from past studies, as it is typically anticipated that flexural strength decreases at this temperature due to the loss of water mass. Similar to the compressive samples, CM samples exhibited superior fire resistance, with a 22.6% drop in flexural strength between the ambient and 600 °C

samples. In contrast, plastic samples exhibited an average 81.3% drop in flexural strength between ambient and 600 °C samples, primarily due to the formation of voids and cracking as the plastic degraded at this temperature.

The failure modes of flexural samples remained consistent across all mix designs at ambient, 100 °C, and 300 °C, with clean cracking forming near the midspan of samples. At 600 °C, plastic samples exhibited unique failure modes due to the degradation of plastics at this temperature, resulting in the formation of voids and cracks in the samples. The failure lines of these samples were inconsistent, rather than forming a smooth crack line observed with other samples below 600 °C. Notably, the stress–deflection curves for plastic samples at 600 °C showed a gradual drop from peak stress rather than an instantaneous drop from peak load, indicating non-brittle failure.

Table 18 The effects of elevated temperature and plastic addition on flexural toughness

Sample type	Post-peak energy $E_{L/m}$ (N.m)	Peak deflection (mm)	PCS ₁₅₀ (MPa)
CM 3DCP ambient direction 'c'	0.211	0.249	0.718
PL5% 3DCP ambient	0.297	0.321	1.163
PL10% 3DCP ambient	0.395	0.406	1.880
PL15% 3DCP ambient	0.227	0.291	0.835
PL20% 3DCP ambient	0.255	0.333	1.024
CM 3DCP 100 °C direction 'c'	0.410	0.427	2.063
PL5% 3DCP 100 °C	0.369	0.371	1.614
PL10% 3DCP 100 °C	0.275	0.255	0.944
PL15% 3DCP 100 °C	0.380	0.276	1.361
PL20% 3DCP 100 °C	0.439	0.417	2.151
CM 3DCP 300 °C direction 'c'	0.500	0.331	1.999
PL5% 3DCP 300 °C	0.723	0.441	3.778
PL10% 3DCP 300 °C	0.725	0.641	8.524
PL15% 3DCP 300 °C	0.675	0.498	4.196
PL20% 3DCP 300 °C	0.805	0.608	7.885
CM 3DCP 600 °C direction 'c'	0.333	0.436	1.716
PL5% 3DCP 600 °C	0.306	0.658	4.038
PL10% 3DCP 600 °C	0.252	0.665	3.493
PL15% 3DCP 600 °C	0.184	0.620	1.921
PL20% 3DCP 600 °C	0.186	0.733	5.205

5 Conclusion

This study utilizes 3DCP technologies with plastic waste as a sustainable aggregate substitute to investigate the mechanical performance and fire resistance of 3D-printed concrete composites incorporating plastics.

- Experimental findings from this study reveal crucial insights into the mechanical properties of 3D-printed concrete with plastic waste. The impact of elevated temperatures on samples was investigated, demonstrating significant mass loss at 300 °C and 600 °C, reaching up to 9.38% and 15.57%, respectively, while minimal mass loss, up to 1.25%, was observed at 100 °C. Specifically, plastic samples exhibited thermal

degradation at 600 °C, resulting in void formation and cracking due to increased internal pressures.

- Inhomogeneity was noted in 3DCP samples, where loading parallel to the layer direction, as opposed to perpendicular, led to an average 51.8% increase in compressive strength and generally higher MOE. Flexural samples from 3DCP showed an average 22.3% increase in flexural strength when the layer direction was parallel to the longitudinal axis of prisms, along with enhanced flexural toughness.
- Comparatively, mold-cast samples demonstrated, on average, a 26% increase in compressive strength over 3DCP samples, exhibiting stiffer behavior characterized by a 42% increase in MOE. However, in flexural samples, mold plastic samples showed a 7.2% decrease in strength compared to 3DCP samples due to the bridging effect. Mold-cast samples, particularly in the absence of plastic, exhibited greater flexural strength, with an average 20.3% increase, and higher ductility as indicated by greater flexural toughness.
- The addition of plastic led to reduced compressive strength compared to CM samples due to its hydrophobic nature, resulting in poor bonding with cement. Both compressive and flexural strengths exhibited a gradual decrease with increasing plastic content across all temperature ranges, although PL5% demonstrated superior flexural strength at all temperatures excluding 600 °C. CM samples displayed superior fire resistance, with a 7.3% difference in compressive strength between ambient and 600 °C, whereas plastic samples exhibited an average 43.5% drop in compressive strength. In addition, MOE for all CM samples surpassed plastic samples at all temperatures, indicating stiffer and less flexible behavior.
- Flexural strength decreased by 22.6% and 81.3% for CM and plastic samples, respectively, between ambient and 600 °C, highlighting the poor fire performance of plastic samples. Furthermore, plastic samples exhibited higher flexural toughness and ductility at all temperatures except 100 °C, as evidenced by increased PCS150 values.
- The experimental results align well with project objectives and previous studies, except for the unexpected increase in flexural strength at 300 °C.

Table 19 Flexural sample failure modes

	Ambient	100°C
CM		
PL5%		
PL10%		
PL15%		
PL20%		
	300°C	600°C
CM		
PL5%		
PL10%		
PL15%		
PL20%		

Future research in the domain of 3DCP with plastic waste could explore utilizing plastic waste in fiber form to understand differences in mechanical properties. In addition, investigating the workability of concrete mixes containing plastic through slump tests could shed light on its impact on the 3D printing process quality. Moreover, the study of shrinkage cracking, especially with more complex structures, presents an avenue for further investigation. Harnessing sustainable concrete composites with 3D printing technology holds promise for reducing environmental impact and construction costs in the construction industry.

Acknowledgements

This work was supported by School of Engineering, University of Western Australia. The authors would like to express their sincere gratitude to Mr Stephen Naulls, Senior Lab Technician at the University of Western Australia.

Author contributions

Mr Walid Yaqub: formal analysis; investigation; methodology; software; validation; visualization; roles / writing—original draft. Dr Farhad Aslani: funding acquisition; supervision; project administration; resources; conceptualization; methodology; data curation; investigation; visualization; writing—review and editing.

Funding

The project has been funded by Dr. Farhad Aslani at UWA.

Availability of Data and Materials

Data can be available upon reasonable request to the corresponding author.

Declarations

Ethics Approval and Consent to Participate

Not applicable.

Consent for Publication

We hereby provide consent for the publication of the manuscript detailed above.

Competing Interests

The authors declare that they have no known competing financial interests or personal relationships that could have appeared to influence the work reported in this paper.

Received: 4 June 2024 Accepted: 17 September 2024

Published online: 02 December 2024

References

- Ahmad, J., Majidi, A., Elhag, A. B., Deifalla, A. F., Soomro, M., Isleem, H. F., & Qaidi, S. (2022). A step towards sustainable concrete with substitution of plastic waste in concrete: overview on mechanical durability and microstructure analysis. *Crystals (Basel)*, *12*(7), 944. <https://doi.org/10.3390/cryst12070944>
- Ali, K., Qureshi, M. I., Saleem, S., & Khan, S. U. (2021). Effect of waste electronic plastic and silica fume on mechanical properties and thermal performance of concrete. *Construction & Building Materials*, *285*, 122952. <https://doi.org/10.1016/j.conbuildmat.2021.122952>
- Almohana, A. I., Abdulwahid, M. Y., Galobardes, I., Mushtaq, J., & Almojil, S. F. (2022). Producing sustainable concrete with plastic waste: A review. *Environmental Challenges*, *9*, 100626. <https://doi.org/10.1016/j.envc.2022.100626>
- AS 1012.2. (1994). Methods of testing concrete, Method 2: Preparation of concrete mixes in the laboratory. Standards Australia.
- AS3582.3. (1994). Supplementary Cementitious Materials for Use with Portland Cement—Silica Fume. Standards Australia.
- AS 1012.12.1. (1998). Methods of testing concrete, Method 12.1: Determination of mass per unit volume of hardened concrete—Rapid measuring method. Standards Australia.
- AS 1478.1. (2000). Chemical Admixtures for Concrete, Mortar and Grout-Admixtures for Concrete. Standards Australia.
- AS 3582.2. (2001). Supplementary Cementitious Materials for Use with Portland and Blended Cement—Slag—Ground Granulated Iron Blast-furnace. Standards Australia.
- AS 3972. (2010). General Purpose and Blended Cements. Standards Australia.
- AS 1141. (2011). Methods for Sampling and Testing Aggregates. Standards Australia.
- AS 1012.8.1. (2014). Methods of testing concrete, Method 8.1: Method for making and curing concrete—Compression and indirect tensile test specimens. Standards Australia.
- Aslani, F., Dale, R., Hamidi, F., & Valizadeh, A. (2022). Mechanical and shrinkage performance of 3D-printed rubberised engineered cementitious composites. *Construction & Building Materials*, *339*, 127665. <https://doi.org/10.1016/j.conbuildmat.2022.127665>
- Aslani, F., & Kelin, J. (2018). Assessment and development of high-performance fibre-reinforced lightweight self-compacting concrete including recycled crumb rubber aggregates exposed to elevated temperatures. *Journal of Cleaner Production*, *200*, 1009–1025. <https://doi.org/10.1016/j.jclepro.2018.07.323>
- Australian Government. (2021). National Plastics Plan summary. Department of Climate Change, Energy, the Environment and Water. <https://www.dcceew.gov.au/environment/protection/waste/publications/national-plastics-plan-summary>.
- Chawla, S., Varghese, B. S., Chithra, A., Hussain, C. G., Keçili, R., & Hussain, C. M. (2022). Environmental impacts of post-consumer plastic wastes: Treatment technologies towards eco-sustainability and circular economy. *Chemosphere (Oxford)*, *308*, 135867–135867. <https://doi.org/10.1016/j.chemosphere.2022.135867>
- De Schutter, G., Lesage, K., Mechtcherine, V., Nerella, V. N., Habert, G., & Agustí-Juan, I. (2018). Vision of 3D printing with concrete—Technical, economic and environmental potentials. *Cement and Concrete Research*, *112*, 25–36. <https://doi.org/10.1016/j.cemconres.2018.06.001>
- Karthick, K., Kumar, S. S., Karthik, T., Lokesh, K., Harris, T. M. A., Jegan, A. M. A., & Raja, S. (2022). Use of recycled plastic waste in concrete composites: A review. *Melville*. <https://doi.org/10.1063/5.0108652>
- Mohammadhosseini, H., Tahir, M. M., Alyousef, R., Alabduljabbar, H., & Samadi, M. (2019). Effect of elevated temperatures on properties of sustainable concrete composites incorporating waste metalized plastic fibres. *SN Applied Sciences*, *1*(11), 1520. <https://doi.org/10.1007/s42452-019-1587-9>
- Perrot, A. (2019). 3D printing of concrete: State of the art and challenges of the digital construction revolution. *ISTE Ltd*. <https://doi.org/10.1002/978119610755>
- Pešić, N., Živanović, S., Garcia, R., & Papastergiou, P. (2016). Mechanical properties of concrete reinforced with recycled HDPE plastic fibres. *Construction & Building Materials*, *115*, 362–370. <https://doi.org/10.1016/j.conbuildmat.2016.04.050>
- Safi, B., Saidi, M., Aboutaleb, D., & Maallem, M. (2013). The use of plastic waste as fine aggregate in the self-compacting mortars: Effect on physical and mechanical properties. *Construction and Building Materials*, *43*, 436–442. <https://doi.org/10.1016/j.conbuildmat.2013.02.049>
- Sanjayan, J. G., Nazari, A., & Nematollahi, B. (2019). 3D concrete printing technology—construction and building applications. *Elsevier*. <https://doi.org/10.1016/C2017-0-02407-2>
- Saxena, R., Siddique, S., Gupta, T., Sharma, R. K., & Chaudhary, S. (2018). Impact resistance and energy absorption capacity of concrete containing plastic waste. *Construction and Building Materials*, *176*, 415–421. <https://doi.org/10.1016/j.conbuildmat.2018.05.019>
- Shen, M., Huang, W., Chen, M., Song, B., Zeng, G., & Zhang, Y. (2020). (Micro) plastic crisis: Un-ignorable contribution to global greenhouse gas emissions and climate change. *Journal of Cleaner Production*, *254*, 120138. <https://doi.org/10.1016/j.jclepro.2020.120138>

- Singh, R. K., Ruj, B., Sadhukhan, A. K., & Gupta, P. (2019). Thermal degradation of waste plastics under non-sweeping atmosphere: Part 1: Effect of temperature, product optimization, and degradation mechanism. *Journal of Environmental Management*, 239, 395–406. <https://doi.org/10.1016/j.jenvman.2019.03.067>
- Thiyagarajan, S. V. (2013). An experimental study on mechanical properties of waste plastic fiber reinforced concrete. *International Journal of Emerging Trends in Engineering and Development*, 2, 395–401.
- Zahabizadeh, B., Pereira, J., Gonçalves, C., Pereira, E. N. B., & Cunha, V. M. C. F. (2021). Influence of the printing direction and age on the mechanical properties of 3D printed concrete. *Materials and Structures*. <https://doi.org/10.1617/s11527-021-01660-7>
- Zhang, Y., & Aslani, F. (2021). Development of fibre reinforced engineered cementitious composite using polyvinyl alcohol fibre and activated carbon powder for 3D concrete printing. *Construction & Building Materials*, 303, 124453. <https://doi.org/10.1016/j.conbuildmat.2021.124453>

Publisher's Note

Springer Nature remains neutral with regard to jurisdictional claims in published maps and institutional affiliations.

Walid Yaqub is a UWA Master's graduate in the School of Engineering at UWA.

Farhad Aslani is an Associate Professor and the Director of the Materials and Structures Innovation Group in the School of Engineering at UWA.